5-5-2010

Semi-classical approaches to below threshold harmonics

James A. Hostetter

Thesis Advisor: Mette Gaarde

Semi-classical approaches to below threshold harmonics

James A. Hostetter
Department of Physics and Astronomy, Louisiana State University, Baton Rouge, Louisiana 70803-4001, USA
(Dated: May 5, 2010)

I. PREFACE

In the fall of 2008, the attosecond research group at LSU received a set of data from Jun Ye's Group in Boulder, CO that exhibited unexpected characteristics (described in section III-C). By using a fully quantum mechanical model (section IV), we were able to successfully recreate the results theoretically that were seen experimentally. However, while the techniques used provided a correct answer, they provided little insight into what was actually causing the observed behavior. Upon further investigation, it appeared that what was happening was very similar to a well-known phenomenon called high harmonic generation which can be described by an intuitive semi-classical model (Section II). However, this model did not apply to the circumstances of the experiment. My thesis project was to expand this model to recreate the results of the quantum model, and this was done successfully. The work has contributed to a cover article in Nature Physics and has produced a paper focusing on these results that has been submitted to Physical Review A.

II. INTRODUCTION

A. What is harmonic generation?

Harmonic generation (HG) is a process by which odd harmonics of some laser frequency are produced. In the realm of optics, it refers to a very specific method that has been very successful both theoretically and experimentally, with HG being observed and exploited since 1987[1, 2]. It is done by driving a noble gas with an intense laser field of frequency ω to produce harmonics of frequency $(2n+1)\omega$ where n is an integer. Typically, these driving lasers are in the infrared range where the produced harmonics can extend all the way to the extreme ultraviolet (XUV) range, or to harmonics with several hundred times the laser frequency. Radiation of about 1 keV photons has been produced[3].

Harmonic generation is a coherent process which yields harmonics that are temporally coherent and spatially directional. The spectrum produced has a distinctive shape (Fig. 1). The lowest harmonics in the spectrum are produced with large intensities that drop off exponentially, as would be expected from perturbation theory. Following these harmonics is the *plateau*, named so because all of the harmonics produced here are of approximately the same intensity. Beyond the plateau is a sharp drop in production of harmonics called the cutoff [1, 5–7]. Because of the characteristics of the harmonics and the shape of the spectra, they are relatively easy to control for many different purposes.

For example, the spectrum of frequencies in the plateau are all separated by 2ω and are of approximately the same intensity. This makes them ideal for use in generating very short laser pulses. Generally, a broad spectrum

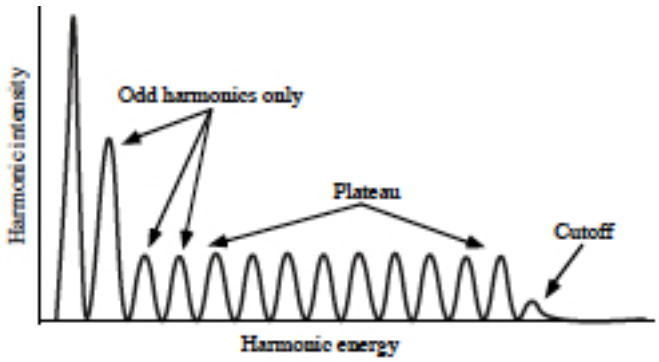

FIG. 1: The characteristic spectrum of HG. [4]

of frequencies can be combined to form a short pulse. The duration of this pulse is inversely proportional to the bandwidth of the spectrum used. Although the harmonics in HG are produced in discrete multiples of the original laser frequency, a pulse of a laser will produce a "chirp" in the frequency that widens the spectral domain of the emission. The large number of plateau harmonics can then be combined in order to produce laser-like XUV pulses of length on the order of a few hundred attoseconds (10^{-18} s). The short wavelength and ultrashort duration of these pulses mean that the harmonic radiation is a very unique source of laser-like XUV radiation. These pulses are ideal for pump-probe type experiments studying the dynamics of electronic processes (as a reference, the period of an electron in a hydrogen atom is 150 as). This will undoubtedly lead to great advancements in our understanding of many atomic phenomena, such as auger scattering, and increase our abilities in material science.

B. The 3-step model

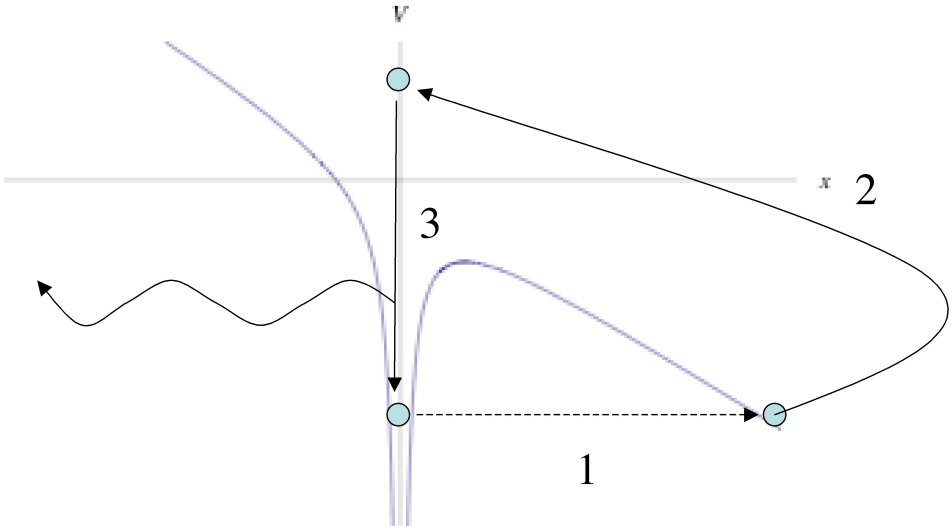

FIG. 2: The standard semi-classical model. (1) The electron tunnels through the combined atomic and laser potentials. (2) The electron is accelerated by the laser field. (3) The electron recombines and releases its energy as a photon.

HG can most easily be explained using a 3-step model proposed in 1993[8, 9]. This model begins with an atomic potential that has been warped by a strong laser field (Fig. 2), allowing an electron bound to the atom to begin a trajectory that can be divided into three parts. First, it may tunnel away from the nucleus. The second step is for the electron to oscillate in and be accelerated by the laser field, giving it extra energy. For electrons that are released between 0.25 and 0.5 laser cycles or 0.75 and 1.0 cycle, return to the parent atom is possible. For the other release times, the electron will be unable to recombine. The third step is actual recombination upon return. When the electron recombines, the atom emits a photon of energy E_{ph} such that

$$E_{ph} = T + I_p \tag{1}$$

where T is the kinetic energy gained from the laser and I_p is the ionization potential. Every half cycle of the laser field, this process starts over. Because of this half-cycle periodicity the radiation spectrum is not continuous but discrete, with peaks separated by 2ω. These peaks are the harmonics.

From this model, we find that the maximum cutoff energy is given by the maximum kinetic energy that the electron can obtain. There are two possible release times in a half-cycle that can achieve the same energy below the cutoff energy. An intuitive way to understand this is by thinking about the initial "kick" away from the atom that the laser gives. The electron is first pushed away from the parent atom by the laser, giving it a certain amount of energy. When the laser field reverses, the opposing "kick" that it gives in the opposite direction must both sap the electron of the energy it has already been given and return the electron to the parent atom.

For example, if the electron is released at the strongest point in the laser's cycle ($\omega t = \pi/2$), it will be accelerated away from the atom for a quarter of a cycle before the laser's field reverses. It will then take another quarter of a cycle to slow the electron to a velocity of 0 (during which time it will continue to move away from the parent atom), and then another to begin to bring it back. The field will reverse again to begin to slow it, and just before its velocity

reaches 0 once more it will finally return to the parent atom. If it had been released any earlier, it would have had too large of a kick to ever return. Released later, it easily returns because the opposing kick is stronger than the initial one.

A *trajectory* is characterized by a specific time of release, which then determines its return time and energy. The two trajectories that produce a given energy are called the *long* and *short* trajectories. The long trajectory is released early in the laser cycle from 0.25 to 0.3 cycles. Because the field is strongest at these release times, the electron travels far and fast from the parent atom. By the time it returns, its motion is against the laser field, causing it to lose the energy it has gained in its travel. The short trajectories are released between 0.3 and 0.5 cycles. They are released when the field is weaker and therefore travel neither as far nor as quickly. However, when it returns it is moving with the laser field and is driven back to the atom. This is how both trajectories can return with the same energy: one is being slowed from a maximum energy and the other is being accelerated from a minimum energy.

The plateau exists because the probability of electrons returning with those energies is approximately equal until the cutoff energy is reached. This is a surprising result as normal perturbation theory would predict that the probability for each harmonic would drop rapidly with higher return energy. Perturbation theory does not apply here because the laser is too intense to qualify as a weak disturbance in the atomic system.

C. This thesis: Can below threshold harmonics be understood with a semi-classical model?

High harmonic generation is described well by the semi-classical model. However, it is clear that the model by construction cannot explain harmonics with energies less than the atom's ionization potential (or *below threshold harmonics*, found in the lower-order harmonics in Fig. 1): eq. 1 allows only photons with energy greater than I_p. Because of this, it has been suspected that below threshold harmonics are produced by multiphoton ionization and have no continuum dynamics.

They have the potential to be very useful because they are produced in the highest quantity. A recent experiment by Jun Ye's group at University of Colorado-Boulder attempted to use these low-energy harmonics to produce frequency combs because they are both produced in high quantity and easy to work with[10]. Through these attempts, it was discovered that the several harmonics several eV below threshold showed evidence of continuum dynamics, described in more detail in later sections. In an effort to explain this, I have attempted to expand the semi-classical model to include the atomic potential and accurately describe this energy range.

To do this, it is essential to understand the standard semi-classical model. In the following section, I will elaborate on the details of the semi-classical model without the atomic potential. From there, I will describe what adjustments must be made to the model in order to properly account for below threshold returns. In particular, I will discuss how the atomic potential was included into the semi-classical model, both in the equations of motions and in the initial conditions. I will then describe the specific techniques I used in my work and close by offering the results of the calculations thus far.

III. THE STANDARD SEMI-CLASSICAL MODEL REVISITED

A. Initial conditions

For the 3-step model to be as simple as it is, a series of assumptions are needed. During the tunneling step, we first assume that the electron tunnels far from the atom. This allows us to approximate the atomic potential as negligible for the entirety of the electron's journey because so little of its time is spent where the atom has much influence (Fig. 3). Next, we assume that the laser is so powerful that it brings the electron far from its starting position. We approximate its initial position as 0.

The initial conditions for an electron released at t_0 can then be summarized in atomic units ($\hbar = e = m_e = 1$) by

$$U(x,t) = \mathcal{E}(t)x \tag{2}$$

$$x(t_0) = 0 \tag{3}$$

$$p(t_0) = 0 \tag{4}$$

where the electric field $\mathcal{E}(t) = \mathcal{E}_0 \sin(\omega t)$ with frequency ω and amplitude $\mathcal{E}_0$. In this case, it is possible to solve the equations of motion exactly:

$$\dot{p}(t) = -\mathcal{E}_0 \sin \omega t \tag{5}$$

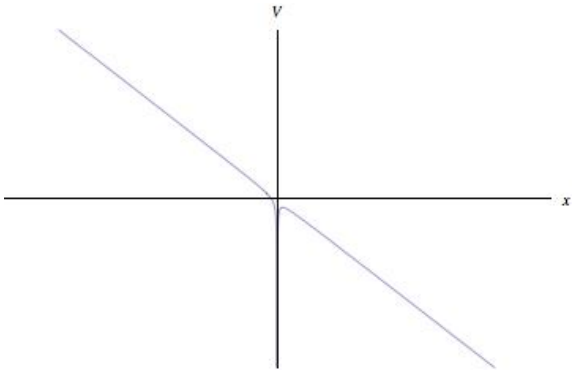

FIG. 3: Zoomed out potential of the laser/atom system. For most of the time spent in the continuum, the electron feels little effect from the atom.

$$p(t) = \frac{\mathcal{E}_0}{\omega}(\cos\omega t - \cos\omega t_0) \tag{6}$$

$$x(t) = \frac{\mathcal{E}_0}{\omega^2}(\sin\omega t - \sin\omega t_0) + \frac{\mathcal{E}_0}{\omega}(t_0\cos\omega t_0 - t\cos\omega t_0) \tag{7}$$

If an electron is released in the first half of the laser cycle ($0 < \omega t_0 < \pi$), it will have an initial negative velocity. If it is released in the second half ($\pi < \omega t_0 < 2\pi$), it will have an initial positive velocity. We are only interested in trajectories that return to $x = 0$ at least once; otherwise, the electron will simply fly into the continuum and never release a photon. Therefore, we need the overall trend of the electron's movement to be opposite in sign to its initial velocity (if the initial velocity is positive, its drift velocity should be negative). Integrating over an entire cycle and dividing by 2π, we see that the average velocity is $-\frac{\mathcal{E}_0}{\omega}\cos\omega t_0$. We discover that for electrons released in the first half of the laser cycle, only those released between 0.25 cycles and 0.5 cycles return. For those released in the second half, only those between 0.75 and an entire cycle return, which is exactly what we wanted to show. Fig. 4 demonstrates the behavior of several release times. To simplify things, we will only discuss electrons released in the first half of a laser cycle.

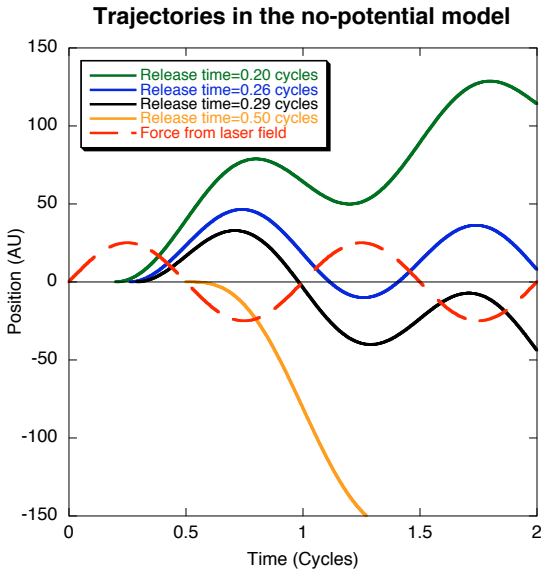

FIG. 4: Trajectories for several release times in the semi-classical model. Electrons released too early (green) or too late (orange) never return to the parent atom from the continuum. Others between 0.25 and 0.5 cycles return one (black) or more (blue) times. The force of the laser on the electron is displayed in arbitrary units.

B. Energy considerations

The equations of motion also lead to the concept of *ponderomotive energy* (U_p), or the cycle-averaged kinetic energy. This directly defines U_p as

$$U_p = \frac{\mathcal{E}_0^2}{4\omega^2} \propto I\lambda^2 \tag{8}$$

U_p is a useful measure of the intensity and wavelength of the laser. By numerically solving the equations of motion, it can be shown with this model that the maximum possible return energy (the *cutoff energy*) is 3.17 U_p. This is consistent with experimental results and fully quantum mechanical calculations [5] showing similar cutoff energies.

C. Phase, action and α

When a harmonic is emitted, it has a phase equal to the phase of the electron whose recombination caused the emission. We can measure the phase and energy of the harmonics experimentally and this allows us to compare our predictions to the real world without having to know where the electron is at all times.

In the semi-classical formulation of quantum mechanics, the phase acquired by the electron wave function is given by the action integral. In the semi-classical model for harmonic generation, this phase is imprinted on to the harmonic radiation produced when the electron returns to the parent atom. If we calculate this phase Φ in such a way, we discover several interesting, measurable properties about the system.

$$\begin{aligned}
\Phi &= \int_{t_0}^{t_r} T - U dt && (9)\\
&= \int_{t_0}^{t_r} \frac{p(t)^2}{2} - \mathcal{E}_0 x \sin\omega t dt && (10)\\
&= \int_{t_0}^{t_r} \frac{p(t)^2}{2} + x\dot{p} dt && (11)\\
&= \int_{t_0}^{t_r} \frac{p(t)^2}{2} dt + xp|_{t_0}^{t_r} - \int_{t_0}^{t_r} p^2 dt && (12)
\end{aligned}$$

where the last line is obtained by integration by parts. We can eliminate the term $xp|_{t_0}^{t_r}$ because $x = 0$ at both t_0 and t_r. Thus,

$$\begin{aligned}
\Phi &= -\int_{t_0}^{t_r} \frac{p(t)^2}{2} dt && (13)\\
&= -\frac{\mathcal{E}_0^2}{\omega^2} \int_{t_0}^{t_r} \frac{\cos^2\omega t - 2\cos\omega t \cos\omega t_0 + \cos\omega {t_0}^2}{2} dt && (14)
\end{aligned}$$

For all of the trajectories in the model, $\Phi \propto U_p/\omega$ because of the $\mathcal{E}_0^2/\omega^2$ contribution. In this way, we see that the phase acquired is both dependent linearly on the intensity and non-linearly on the release time of the electron. This is important because it provides us with a direct way to measure the accuracy of the predictions of this semi-classical model. We define a unitless value α such that

$$\alpha = -\frac{\Phi\omega}{U_p} \tag{15}$$

where the integral has been absorbed into α as a constant.

There are several characteristics of α to identify. First, α is proportional to the phase, giving it a larger value with greater time spent in the continuum under the laser's influence. However, while the phase increases with increasing laser intensity and longer wavelengths, the U_p and ω contributions cancel these effects for α. Thus, α is solely a function of travel time and not of intensity. This affords us another way of distinguishing long and short trajectories: for any given return energy, the trajectory with the larger α is the long one. Depending on the return energy, α varies between zero and π for the short trajectory and between π and 2π for the long trajectory.

Equation 15 is also useful rearranged as

$$\Phi = -\frac{\alpha U_p}{\omega} \tag{16}$$

With this formulation, we see that, as ω is constant, α is actually the slope of how the phase changes with intensity. The intensity-dependent phase is an important concept in harmonic generation. Since α is different for the short and long trajectories, at each intensity they contribute different phases to the dipole, producing oscillations in the harmonic intensity as a function of laser intensity due to interference between the long and short trajectories. Additionally, we may imagine initiating HG with a femtosecond laser pulse characterized by an intensity $I(r, z, t)$. Because the laser intensity depends on time, the intensity dependence of the phase gives rise to a spectral broadening of each harmonic. This one pulse contains many individual laser cycles. Because each cycle will cause two sets of returns, we end up with many emissions of light from similar trajectories with different phases. This induces a change in the frequency of any harmonic produced equal to $\Delta\omega(t) = -\partial\Phi(t)/\partial t$ called the *chirp*, leading to the spectrum of the emission around that harmonic to broaden. By measuring the width of this spectrum, we can determine how the phase is changing with respect to intensity and compare it to theoretical predictions.

A third effect that the intensity dependent phase has is to create a distinctive spatial profile for the emitted harmonic. The laser beam varies radially in intensity. Such a variation introduces a curved phase front to the emission of a harmonic, which in turn produces a strongly divergent beam for those harmonics that are produced under high intensity or with large α. Each harmonic has one short trajectory with small intensity-dependent phase and one long trajectory with large intensity-dependent phase, so the profile of the beam is the superposition of one collimated beam from the short trajectory and one divergent beam from the long trajectory, producing a halo effect. Both the halos in the spatial distribution and the spectral bandwidths have been experimentally measured in high order harmonics and found to be in good agreement with theoretical predictions [11, 12]. More recently, Yost et. al have found these same behaviors in below threshold harmonics [10], leading to our current investigation.

IV. QUANTUM PATH DISTRIBUTIONS FOR LOW ORDER HARMONICS

I will begin by describing a technique commonly used for analyzing phase information in fully quantum mechanical calculations. This method was used by a post-doc in our group, Jennifer Tate, to study the data from Jun Ye's group and later the data resulting from my calculations. This technique was not performed by me, but it is well-known in the field[13, 14].

All of the elements of the semi-classical model can be recognized in a fully quantum mechanical model based on numerical integration of the time-dependent Schödinger equation (TDSE)[5]. The process of harmonic generation results from the creation of a time-dependent dipole moment that has Fourier components at frequencies $q\omega$ where q is an odd integer and ω is the driving laser frequency. We discussed above, that in the standard semi-classical model of high harmonic generation, this dipole moment at the q^{th} harmonic, d_q is first written as a sum over a small number of contributions each characterized by a phase S_q^j and coefficient a_j

$$d_q(I) \sim \sum_j a_j \, e^{iS_q^j}. \tag{17}$$

The different j contributions are the trajectories discussed above, and the phase S_q^j is simply the classical action.

To make the connection between full quantum mechanical calculations and this semi-classical picture, we begin by writing the full intensity-dependent phase $d_q(I)$ as the sum of contributions characterized by a parameter α that is conjugate to the intensity:

$$d_q(I) = \int \tilde{d}_q(\alpha) e^{-i\alpha U_p(I)/\omega} d\alpha. \tag{18}$$

We then attempt to extract the dominant phase contributions to d_q from a full quantum mechanical calculation and compare them with the semi-classical phases α_j. We do this by calculating the complex intensity-dependent d_q via numerical integration of the TDSE. We solve the TDSE for a hydrogen atom interacting with an intense 1070 nm laser field with a quasi-constant peak intensity, and we do this for many different intensities. For each harmonic q, and each intensity I_0, we then analyze the intensity dependent dipole moment $d_q(I_0)$ in terms of the conjugate phase variable α, as described in [13]:

$$\tilde{d}_q(\alpha, I_0) = \int d_q(I) e^{i\alpha U_p(I)/\omega} W(I - I_0) dI \tag{19}$$

where $W(I - I_0)$ is the same window function centered on I_0 used in [13]. For above-threshold harmonics, the phase coefficients obtained in this way from the full quantum calculations correspond well to those predicted by the semi-classical model [13].

These types of calculations have also had success in describing real results from where below threshold harmonics showed several characteristics of high harmonic generation, like in the Yost et al measurements [10]. Fig. 5 shows such signatures compared with the calculated intensity dependent yields. The calculations include both the microscopic quantum mechanical response and the collective response of the macroscopic number of atoms in the gas [10]. The steps in the intensity dependent yield and the haloes on the spatial distributions both indicate that there are multiple contributions to these harmonics with different intensity dependent phases. In [10] we performed our calculated results and found that there were indeed several quantum paths contributing to these low order harmonics. In this thesis, we try to understand this behavior in terms of a generalized semi-classical model.

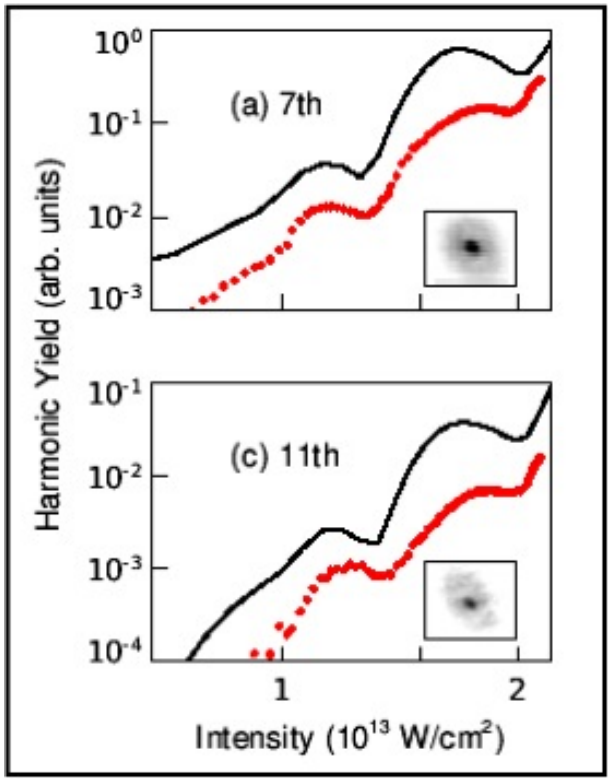

FIG. 5: Halos in the harmonic profile (inset) and steps in the harmonic intensity are found in the 7th and 11th below threshold harmonics in experiment (red). The steps are successfully reproduced by the real calculations (black).[10]

Yost et. al measured low order harmonics in xenon. In this thesis we have concentrated on hydrogen since because of the simplicity in comparing the hydrogen system to the semi-classical model. Fig. 6 shows the calculated quantum path distributions for harmonics 7, 9, 11, and 13 in hydrogen. Each of the vertical stripes represent different α. From the figure, it is clear that all four have two contributions: one near (and sometimes less than) zero and one slightly greater than 2π. These are the results that I will be trying to replicate with a generalized semi-classical model.

V. GENERALIZED SEMI-CLASSICAL MODEL

As discussed above, our generalization of the semi-classical model involves including the atomic potential into the model. In our attempt to generalize the SCM, we must first decide on what form our atomic potential should take. We must recalculate all of the equations of motion, so our potential should allow us to do that. Because the problem becomes so much more complicated, we cannot solve the problem by direct integration; thus, we use numerical integration. This requires that the potential be smooth and continuous, so we cannot use the simple $-\frac{1}{|x|}$. We instead use

$$U_{at}(x) = -\frac{1}{\sqrt{x^2 + a^2}} \tag{20}$$

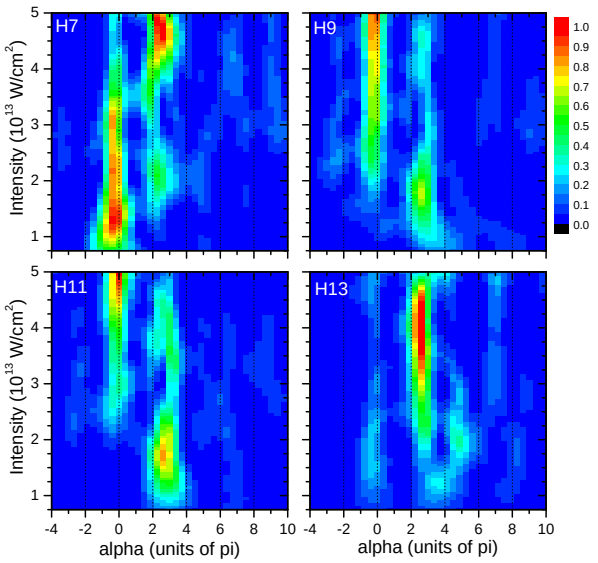

FIG. 6: Quantum path distributions for (below threshold) harmonics 7 through 13 in hydrogen.

where the size of the constant a controls the strength of the potential well. We usually say that $a = \frac{1}{U_0}$, where U_0 is the so-called "well depth" because -U_0 is the lowest point in the well. A larger U_0 leads to a deeper well (or a stronger atomic potential). The atomic potential combined with the laser potential is then

$$U(x) = U_{laser} + U_{at} = xE_0 \sin\omega t - \frac{1}{\sqrt{x^2 + a^2}} \tag{21}$$

and our equation of force then becomes

$$\dot{p} = \sin\omega t - \frac{x}{(x^2 + a^2)^{3/2}} \tag{22}$$

which has equations of motions that are not solvable directly.

Because an electron placed in this "well" will never escape the potential if given the initial conditions found in eq. 3 and eq. 4, we must develop a new set of initial conditions. There are two basic models that we use to do this: the tunneling model and the OTB model.

A. Tunneling Model

The initial conditions closest to that of the standard SCM are given by releasing the electron via tunneling through the potential barrier formed by the combined laser and atomic potential, with $x(t_0) \neq 0$ and $p(t_0) = 0$. We estimate $x(t_0)$ using a simplified Coulomb potential $U_{at}(x) = -1/|x|$ and finding where the combined potential equals the ionization potential outside of the barrier, which yields:

$$x(t_0) = \frac{I_p + \sqrt{I_p^2 - 4|\mathcal{E}(t_0)|}}{2|\mathcal{E}(t_0)|} \tag{23}$$

$$p(t_0) = 0 \tag{24}$$

where I_p is $U_0/\sqrt{2}$. In the results section, we will refer to these trajectories as tunneling trajectories. To prevent extremely unlikely (large) tunneling distances, we filtered out all results with initial positions greater than 25 au. We also filtered imaginary results (where $I_p^2 - 4|\mathcal{E}(t_0)|$) as they correspond to the ionization potential of the electron being higher than the potential "barrier" seen in Fig. 7 and thus are no longer compatible with the concept of tunneling.

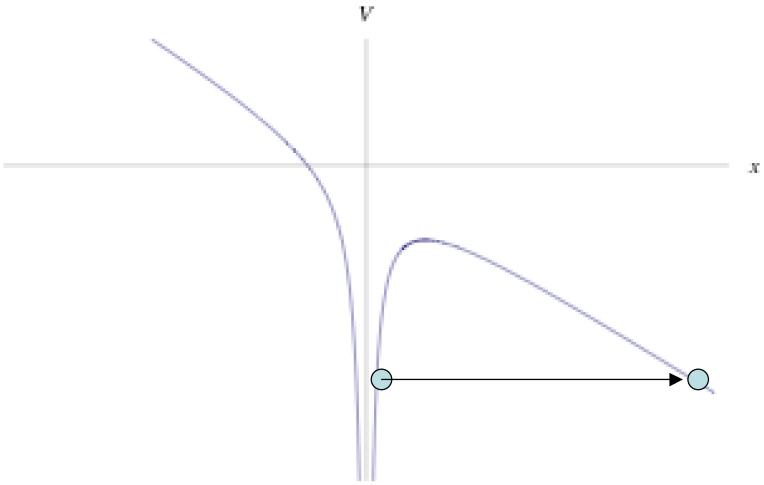

FIG. 7: Graphic representation of the initial conditions for the tunneling model.

B. Over the Barrier

Another approach that can lead to below threshold harmonics is to allow the electron a classical over-the-barrier (OTB) escape. Here we assume that the electron has been excited to some energy E while at $x = 0$, similar to multiphoton ionization. In other words, we create the initial conditions

$$x(t_0) = 0 \tag{25}$$

$$p(t_0) = \pm\sqrt{2(E + U_0)} \tag{26}$$

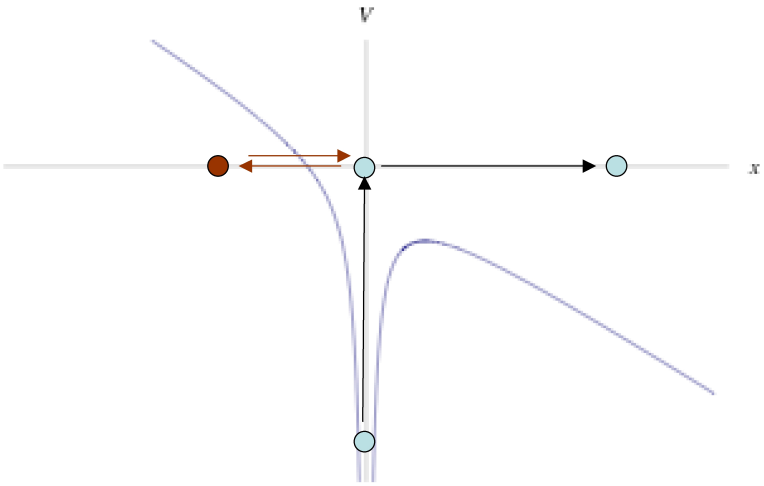

FIG. 8: Graphic representation of the initial conditions for the OTB model.

This gives rise to two possible classes of trajectories for the electron. The first occurs when the electron first moves "downhill" in the warped potential. The electron spends its energy going over the potential bump caused by the distortion in the atomic potential by the laser. It is then mostly free from the atomic potential and has an extra "kick" behind it that influences whether it returns and should it, with how much energy.

The second class of trajectories occurs when the electron initially moves against the potential wall caused by the addition of the atomic and laser potentials. These "uphill" trajectories return almost immediately to $x = 0$ and then continue to follow a trajectory similar to that of the first class.

There are two reasonable energy limits for the OTB initial conditions. Our upper limit is $E = 0$, which gives the electron enough energy to escape the atom in the absence of the laser potential. Our lower limit is $E_{min} = -2\sqrt{|\mathcal{E}(t_0)|}$, or the maximum height of the barrier at the time of release. Since the electron has a finite velocity and the height of the barrier is constantly changing, the electron will have either an excess or deficiency of energy when encountering the barrier. On a deficiency, the electron will simply return and produce a low α return. We allow the electron to be released with any energy between these two limits, and thus consider a range of different trajectories within this type of initial condition.

C. Trajectories and achievable energies

The long and short trajectories evolve in response to the changes in initial conditions and potential. In the tunneling model, we find that below threshold long trajectories can exist, but not below threshold short trajectories. In the OTB model, there are below threshold results for both the long and short trajectories.

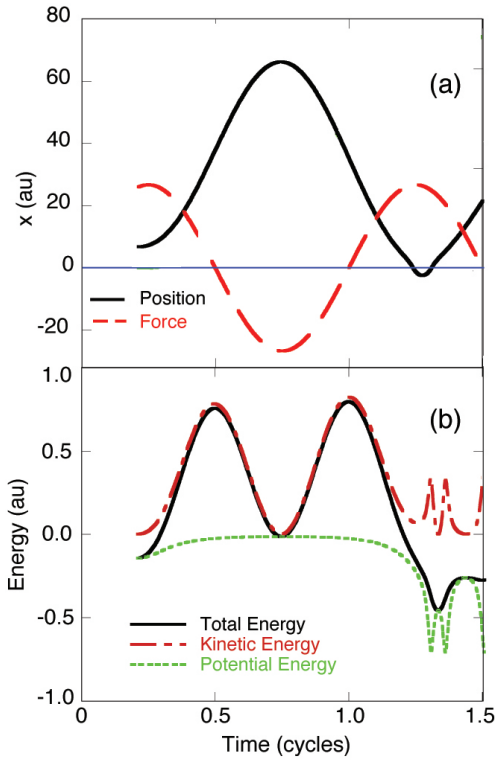

FIG. 9: (color online) Long trajectory dynamics in the tunneling-initiated generalized SCM: a) Position versus time. Dashed (red) lines represent the force from the laser field. b) Energy versus time of the identical trajectory. The intensity is 10^{14} W/cm^2 the return energy is -.25 au, which corresponds to -.58 U_p, or approximately the 7th harmonic.

The electron dynamics leading to long-trajectory below threshold return energies in the tunneling model are illustrated in Fig. 9. In (a) we show the trajectory and in (b) we show the evolution of the kinetic and potential energy with time. In the no-potential model the electron along this trajectory would barely miss recombination because it would be returning with insufficient energy at a time when the laser field is against its motion. In our case, the atomic potential overcomes the field and pulls it (slowly, due to the opposing field) into the atom. This is easily seen in the returns in Fig. 9(b), indicated by peaks in the kinetic energy and minimums in potential energy. In the OTB model (not shown in Fig. 9), downhill trajectories are released into the continuum (at $x_0 = 0$) already traveling with some initial velocity away from the core and behave very similarly to the tunneling trajectories, in that they can lead to long trajectory below-threshold returns.

The absence of low-energy returns for the short trajectory initiated by tunneling in the generalized SCM is illustrated

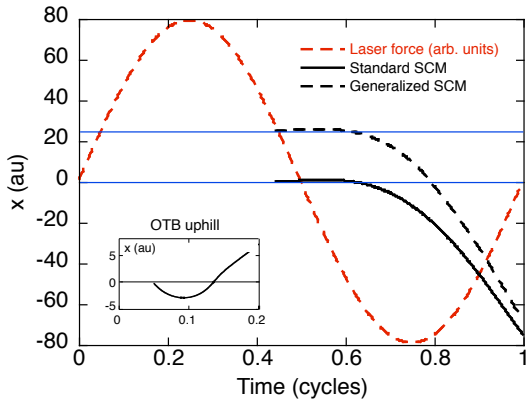

FIG. 10: (color online) Dynamics of the short trajectory initiated by tunneling, in the standard (solid black line) or generalized (dashed black line) SCM. Red dashed lines represent the force from the laser field. Inset: Uphill trajectory of the OTB model.

in Fig. 10. The solid line shows a standard SCM low-energy short trajectory, which is released when the laser field is weak and spends only a very short time away from the core before returning with low energy. In our generalized SCM (dashed line) the electron must tunnel very far when the laser field is weak and therefore must travel a long way to return back to the ion core, during which it is accelerated by the laser field (and by the attractive atomic potential) and returns with high energy. Thus, one difference between the short and long trajectories while including the atomic potential is whether or not the electron is being accelerated by the laser as it recombines (short trajectory) or slowed (long trajectory).

The electrons initially moving uphill in the OTB model can follow qualitatively different trajectories. In particular, such initial conditions allow for very short trajectories with below threshold return energies in which the electron simply scatters off of the potential and immediately returns (seen in the inset of Fig. 10). There are even a few downhill OTB trajectories which can lead to below threshold short trajectories when we allow the initial energy of release to be low (usually near E_{min}). These electrons can be pulled back to the core by the atomic potential if they are released in a very weak field.

D. Phase

An important question of this new potential arises. If we include the potential, can we still accurately describe its behavior with this semi-classical model at all? To answer this, we first turn to the way that we predicted measurable properties with the no-potential case where we were able to predict changes in phase with changes in intensity. In our definition of phase, U is no longer simply the laser potential and therefore $\dot{p} = -\mathcal{E}_0 \sin\omega t - \frac{\partial U_{at}}{\partial x}$ (or $\dot{p} + \frac{\partial U_{at}}{\partial x} = -\mathcal{E}_0 \sin\omega t$)

$$\Phi = \int_{t_0}^{t_r} T - U dt \tag{27}$$

$$= \int_{t_0}^{t_r} \frac{p(t)^2}{2} - \mathcal{E}_0 x \sin\omega t - U_{at} dt \tag{28}$$

$$= \int_{t_0}^{t_r} \frac{p(t)^2}{2} + x\dot{p} + x\frac{\partial U_{at}}{\partial x} - U_{at} dt \tag{29}$$

$$= \int_{t_0}^{t_r} -\frac{p(t)^2}{2} + x\frac{\partial U}{\partial x} - U_{at} dt \tag{30}$$

$$= \int_{t_0}^{t_r} -\frac{p(t)^2}{2} + \frac{x^2}{(x^2+a^2)^{3/2}} + \frac{1}{\sqrt{x^2+a^2}} dt \tag{31}$$

$$= \int_{t_0}^{t_r} -\frac{p(t)^2}{2} + \frac{2x^2+a^2}{(x^2+a^2)^{3/2}} dt \tag{32}$$

This no longer has a simple relation to intensity. While the first term is the same, the second now makes it very difficult to predict how any given electron's phase will be affected by the intensity. The first only subtracts from

the phase and is greatest when the electron is moving fastest. The second is always positive and is greatest near the parent atom. The phase is now a competition between the well depth and the intensity, making it non-trivial to predict. We must perform more advanced calculations to make any predictions, described in the next section.

VI. TECHNIQUES

To calculate all of the data, I coded in FORTRAN 90. I found the equations of motion and phase by numerically integrating equations 22 and 32 using the Runge-Kutte method of integration. In running this program, each trajectory had several free parameters to choose, presented in the table below:

Intensity of driving laser	$0.2 - 5.96$ x 10^{13} W/cm^2
Wavelength of the driving laser	1070 nm
Release time of the electron	0.00-0.5 laser cycles
Depth of the atomic potential	$1/\sqrt{2}$ (Hydrogen-like)
Ionization potential	0.5 (Hydrogen-like)

The choice of parameters was chosen to best represent hydrogen, the simplest possible system available. For one "run" of trajectories, I picked a constant intensity and then looped through many possible release times, recording the results of each.

In order to calculate α correctly, I refer back to the definition of the change in phase as a function of U_p/ω (eq. 16). Since the phase is no longer directly proportional to the intensity, we cannot calculate α as $-\frac{\Phi/\omega}{U_p}$. Instead we define the instantaneous α as $-d\Phi/d(U_p/\omega)$, which must be numerically evaluated. To find the instantaneous α for a harmonic at a given intensity then requires a numerical calculation of $-d\Phi/d(U_p/\omega)$. Because each energy can be formed by two trajectories in the no-potential case, it is important to differentiate between the long and short trajectories by return time t_r. We may use the definition of α

$$\alpha(t_r, I_0) = -\frac{d\Phi}{d(U_p/\omega)} = -\frac{\Phi(t_r, I_0+\delta I) - \Phi(t_r, I_0-\delta I)}{\Delta(U_p/\omega)} \tag{33}$$

$$= -(\frac{1}{U_p/\omega})\frac{S(I_0+\delta I) - S(I_0-\delta I)}{2\delta I/I_0} \tag{34}$$

To calculate this, I ran sets of trajectories for two intensities that surrounded a central intensity I_0 by δI =0.1I. Each harmonic was distinguished by first interpolating what its return time was at intensity I and using the same return time to find the action at the surrounding intensities. Fig. 11b demonstrates the results of this technique as a proof of concept.

Fig. 11a shows that the phase components likely to lead to something like a long trajectory are fairly similar for all three initial conditions, meaning that there are many ways to achieve the long trajectory dynamics that we see in the experimental data. We also see that only the uphill OTB model creates anything that resembles a below threshold short trajectory, as the downhill OTB and tunneling models do not have any low-energy returns with a small phase. An interesting consequence of changing the initial conditions is that the tunneling model has a larger cutoff energy than the OTB models. The phase is overall less than the SCM because of the atomic component of the phase equation. This also allows a negative phase, unseen until now. The energy distribution is continuous because the discreteness of the spectrum in Fig. 1 is caused by a quantum mechanical effect.

However, this approach is difficult to do at the many different intensities that are required to compare to the quantum path calculations. Immediate difficulties include calculating data points densely enough to interpolate reliably, but not so dense as to slow the program to a crawl when it must calculate not just the intensity we are interested in but also the two surrounding intensities. Another barrier is that different models for release will not behave like the no-potential model and may exhibit unexpected qualities that interfere with our basic assumptions. For example, in both the tunneling model and the uphill OTB model, several different harmonics may have similar return times that must be distinguished. All of these quirks would have to be well-known and compensated for for a range of intensities.

A simpler and perhaps more accurate way of comparing the two is to interpolate the phase of each harmonic and input that data directly into the window algorithm for direct comparison. To do this, we first simulate the trajectories for many release times. We then isolate the first returns of each trajectory and find two that have energies surrounding the energy of the harmonic we wish to study. By using the phase of these returns to interpolate what phase the exact harmonic would have, we obtain one contribution for the different phase components. We can repeat this process to

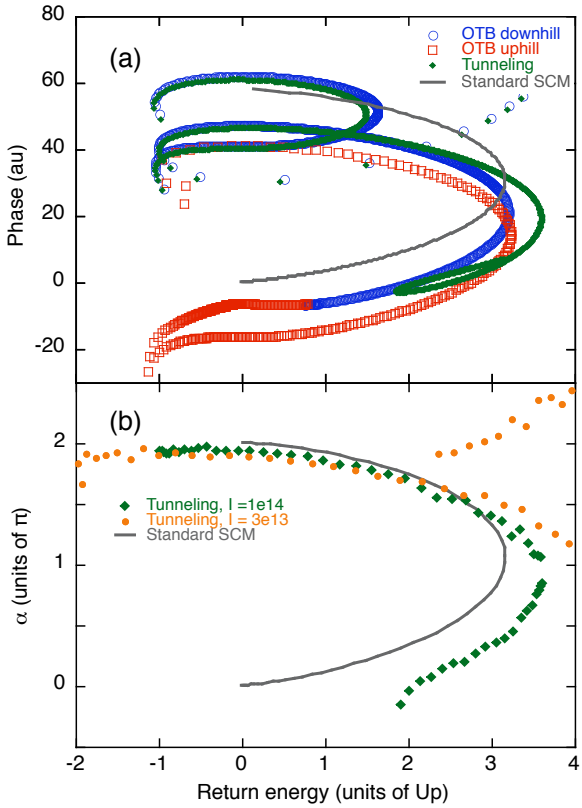

FIG. 11: a) -Φ accumulated at 10^{14}W/cm^2 for the different models. b) Instantaneous α calculated at several intensities in the tunneling model. Below threshold trajectories have return energy less than 0.

find a second phase component. These two phase components are the contributions from the modified short and long trajectory. We also perform this analysis on the second returns. We do this over the same range and interval as the previous calculations so that we may use the same window technique to compare the data. In our case, the range of intensities that were used was 0.2-5.96 x 10^{13} W/cm^2.

VII. RESULTS

A. Tunneling Model

Fig. 12 shows the quantum path distribution of the dipole moment constructed using the tunneling model. As we expected, there is no $\alpha = 0$ contribution from this model because there is no way for the electron to have both a low energy and a small travel time. However, we do observe strong contribution around 2π, indicating something analogous to above threshold long trajectories. These contributions increase with decreasing intensity, an effect that is also seen in the fully quantum calculations. Not shown are the individual phase components that lead to this overall picture. Some of these components are above 2π and some are below, leading to one very strong contribution at 2π.

B. OTB Model

Figs. 13 and 14 show the results of the OTB model for $E_{init} = 0$ and $E_{init} = E_{min}$. As discussed earlier, the downhill results look very similar to the tunneling results. The main difference is the intensity at which returns give results at these energies. This is because at intensities that are too small, the distance that the electron would have to tunnel is too large and so those calculations are skipped. Other than that, we know already that the electron trajectories are very similar for both the downhill and tunneling models. The maximum and minimum energy pictures

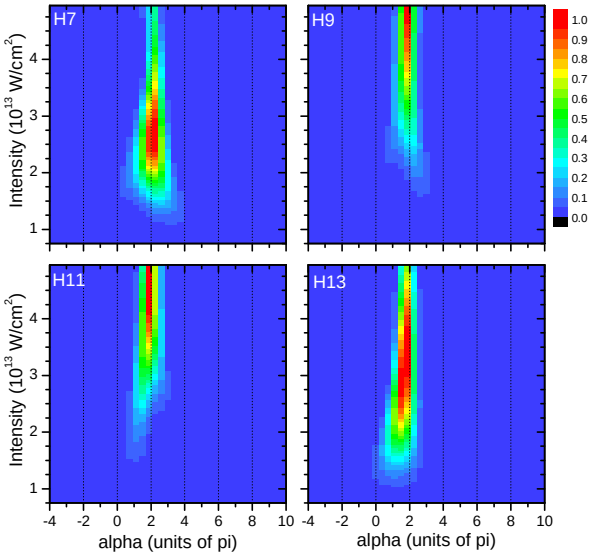

FIG. 12: Quantum path results for Tunneling model.

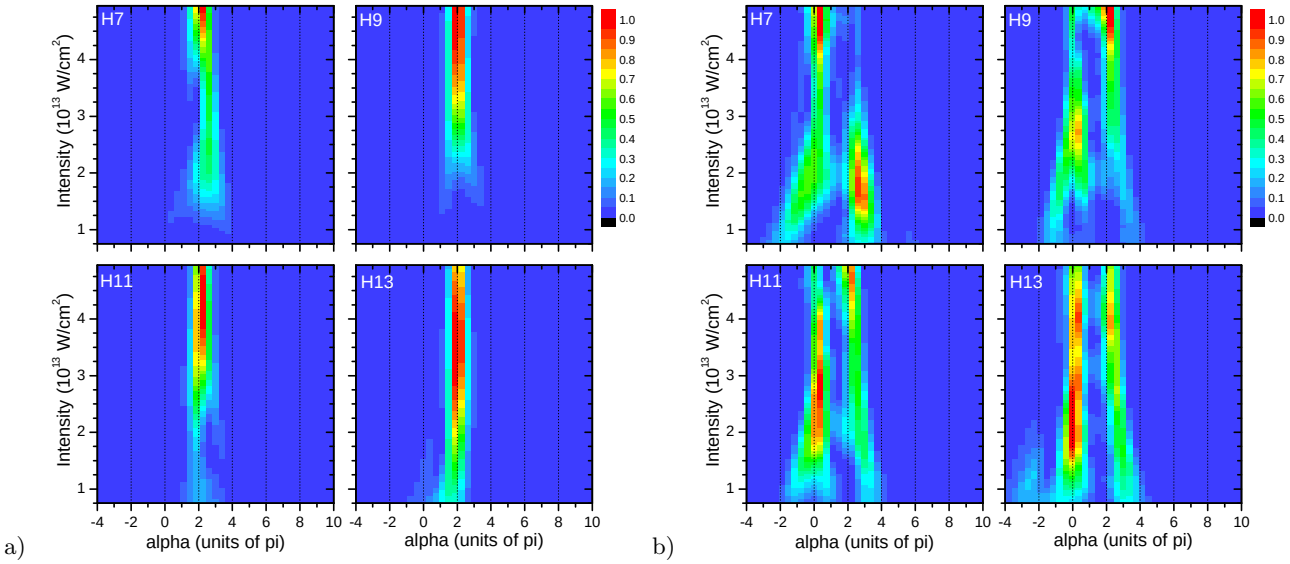

FIG. 13: Quantum path results for maximum energy allowed in OTB model. a) is downhill. b) is uphill.

provide a kind of upper and lower limit for the values of α. The actual expected results should be considered to be some sort of intermediate between the two.

The uphill trajectories are the only ones that contribute an $\alpha \approx 0$ component. We show how it is possible to obtain a negative α component, unseen before now. The short trajectory also becomes more negative at intensity decreases, a trend also seen in fully quantum calculations. They also show the increase in α with decreasing intensity in the long trajectory that the other models show.

VIII. SUMMARY

We have presented one approach to generalizing the semi-classical three-step model of harmonic generation, in which we have included the effects of the atomic potential in both the continuum dynamics of the electron, and in the initial

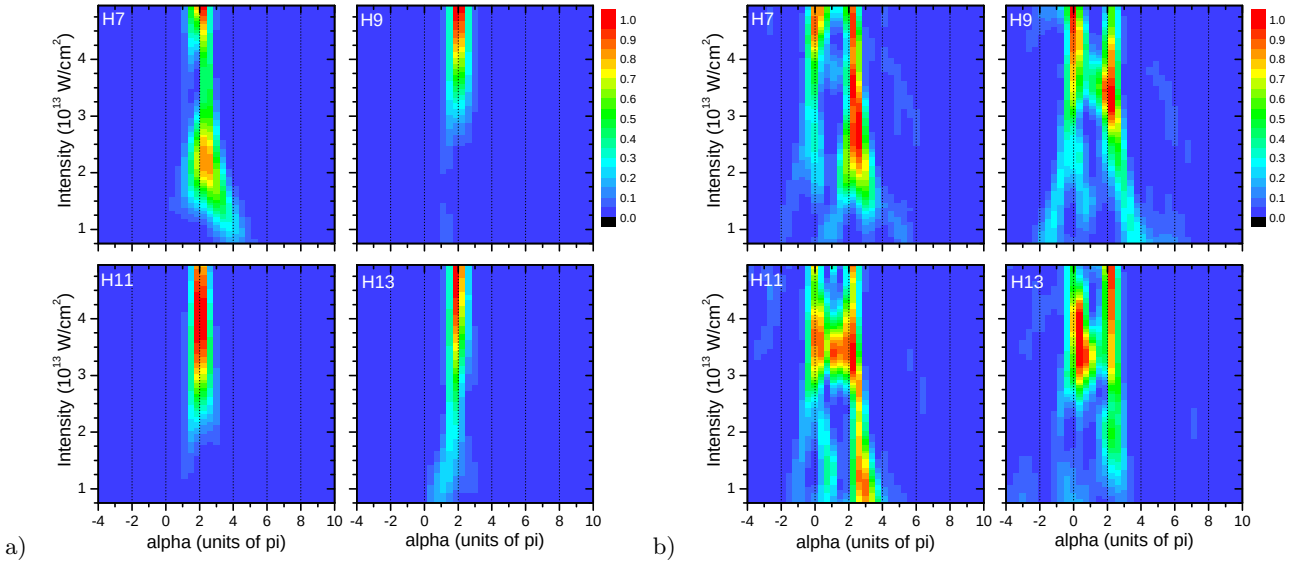

FIG. 14: Quantum path results for minimum energy allowed in OTB model. a) is downhill. b) is uphill.

ionization process. For the continuum dynamics, we included the atomic potential simply by solving the classical equations of motion for an electron moving in the combined laser/atomic potentials. For the ionization process we included the atomic potential via the choice of initial conditions, which we chose to mimic either (i) tunnel ionization, by releasing the electron outside the laser-induced potential barrier with zero velocity, or (ii) multiphoton ionization, by releasing the electron at the ion core with non-zero kinetic energy, moving either uphill or downhill with respect to the laser potential.

We calculated the intensity-dependent phase accumulated along the generalized semi-classical trajectories and found results in good agreement with a range of experimental measurements, as well as with fully quantum mechanical calculations in hydrogen. In particular, we found that there are semi-classical trajectories leading to return energies that are below the ionization threshold of our model atom, in agreement with the experimental observation of semi-classical dynamics in below threshold harmonics in xenon [10]. We showed that the long trajectory readily generalizes and is relatively insensitive to the choice of initial conditions. We also showed that there are no low-energy short trajectories initiated by tunneling in the generalized model, simply because tunneling releases the electron far from the core and it is subsequently accelerated all the way back by both the laser and the atomic potential. In contrast, the low energy electrons returning along the long trajectory move against the laser field when they are close to the core, and can end up with below threshold energies because they get "pulled in" by the attractive atomic potential. Finally, we showed that the short-trajectory characteristics well known from the standard SCM can be reproduced only if the electron is released into the continuum in a process which is closer to multiphoton than to tunnel ionization. These multiphoton-initiated short trajectories can give rise to below threshold harmonics with an intensity dependent phase which has the opposite sign of that observed for high order harmonics.

[1] A. McPherson et. al, J. Opt. Soc. Am. B **4**, 595-601 (1987).
[2] J. Phys B: At. Mol. Opt. Phys **21**, L31-L36 (1988).
[3] L'Huillier et. al., Journal of Nonlinear Optical Physics and Materials **4**, 647-665 (1995).
[4] C. Schaffer, NATO Advanced Study Institute: International school of atomic and molecular spectroscopy, Ed. B., 611-623 (1993).
[5] Krause et. al., Phys. Rev. Lett **68**, 3535 (1992).
[6] Zhou et. al., Phys. Rev. Lett. **76**, 752 (1996).
[7] L'Huillier et. al., Phys. Rev. Lett. **70**, 774 (1996).
[8] K. J. Schafer, B. Yang, L. F. DiMauro, and K. C. Kulander, Phys. Rev. Lett. **70**, 1599 (1993).
[9] P. B. Corkum, Phys. Rev. Lett. **71**, 1994 (1993).
[10] D. C. Yost, T. R. Schibli, J. Ye, J. L. Tate, J. Hostetter, M. B. Gaarde, and K. J. Schafer, Nat. Phys. **5**, 815 (2009).
[11] M. Bellini, C. Lyngå, A. Tozzi, M. B. Gaarde, T. W. Hänsch, A. L'Huillier, and C. -G. Wahlström, PHys. Rev. Lett. **81**,

297 (1998).
[12] Y. Mairesse, A. de Bohan, L. J. Frasinski, H. Merdji, L. C. Dinu, P. Monticourt, P. Breger, M. Kovaĉev, R. Taíeb, B. Carré, H. G. Muller, P. Agostini, P. Salières, Science **302**, 1540 (2003).
[13] Balcou, Ph., Dederichs, A. S., Gaarde, M. B., & L'Huillier A. Quantum-path analysis and phase matching of high-order harmonic generation and high-order frequency mixing processes in strong laser fields. *J. Phys. B* **32**, 2973 (1999).
[14] Gaarde, M. B., & Schafer, K. J. Quantum path distributions for high-order harmonics in rare gas atoms. *Phys. Rev. A* **65**, 031406(R) (2002).